

Enabling Real-Time Colonoscopic Polyp Segmentation on Commodity CPUs via Ultra-Lightweight Architecture

Weihao Gao^{1,*}, Zhuo Deng², Zheng Gong², Lan Ma²

¹School of Computer Science and Artificial Intelligence, Guangdong University of Education

²Shenzhen International Graduate School, Tsinghua University

Abstract

Early detection of colorectal cancer hinges on real-time, accurate polyp identification and resection. Yet current high-precision segmentation models rely on GPUs, making them impractical to deploy in primary hospitals, mobile endoscopy units, or capsule robots. To bridge this gap, we present the UltraSeg family, operating in an extreme-compression regime (< 0.3 M parameters). UltraSeg-108K (0.108 M parameters) is optimized for single-center data, while UltraSeg-130K (0.13 M parameters) generalizes to multi-center, multi-modal images. By jointly optimizing encoder-decoder widths, incorporating constrained dilated convolutions to enlarge receptive fields, and integrating a cross-layer lightweight fusion module, the models achieve ≥90 FPS on a single CPU core without sacrificing accuracy. Evaluated on seven public datasets, UltraSeg retains >94% of the Dice score of a 31 M-parameter U-Net while utilizing only 0.4% of its parameters, establishing a strong, clinically viable baseline for the extreme-compression domain and offering an immediately deployable solution for resource-constrained settings. This work provides not only a CPU-native solution for colonoscopy but also a reproducible blueprint for broader minimally invasive surgical vision applications. Source code is publicly available to ensure reproducibility and facilitate future benchmarking.

1. Introduction

Colorectal cancer often arises from the malignant transformation of colorectal polyps, and both its incidence and mortality remain high [24]. Colonoscopy, the primary screening modality for these polyps, allows direct visualization of their morphology and facilitates the resection of malignant lesions [6,30]. However, the intricate anatomy of the colon frequently causes polyps to be missed. Recent work has explored image-classification or object-detection tech-

niques to assist real-time video interpretation [1, 19, 20, 33], yet polyp **boundary segmentation** goes further: it supplies pixel-level location and contour information, provides richer visual cues for intra-operative resection, and enables models to learn deeper pixel-wise representations of polyps, thereby boosting the performance of downstream diagnostic tasks [12]. Accurate polyp segmentation is therefore essential for the early diagnosis of colorectal cancer.

Nevertheless, polyp segmentation remains a complex and challenging task. Polyps often exhibit indistinct boundaries and highly variable size and morphology, giving them strong camouflage characteristics [18]. Traditional manual segmentation relies on the clinician’s subjective experience and sustained attention, resulting in limited consistency. Early computer-assisted methods predominantly exploited low-level features such as shape, texture, or color; although fast, their accuracy and robustness are insufficient when the contrast between polyps and surrounding mucosa is low [3].

In recent years, convolutional neural networks (CNNs)—a cornerstone of deep learning—have drawn substantial attention for polyp segmentation. Among them, U-Net stands out as the most representative architecture; its elegant design and compelling performance have made it a de facto standard in medical image segmentation [28]. As deep learning evolves, emerging backbones such as Transformer and Mamba have also been transplanted to this field, yet the accompanying surge in parameters often compromises clinical deployability [9, 10, 13].

Accurate polyp segmentation is pivotal for early cancer diagnosis; however, several critical challenges persist in automated workflows. First, inter-scanner variability—stemming from differences in imaging processors and light sources across manufacturers (e.g., Olympus, Pentax, Fujifilm)—renders the same lesion markedly divergent in color, texture, and geometric distortion. Models trained on one device therefore suffer pronounced performance drops when transferred to another. Second, the coexistence of white-light endoscopy (WLE), narrow-band imaging (NBI),

*Corresponding author. Email: weihaomeva@163.com

blue-laser imaging (BLI), and linked-color imaging (LCI) implies that the same polyp can exhibit drastically different contrast and edge characteristics under distinct spectral modalities, further complicating the extraction of universal features [17].

On the other hand, real-time colonoscopy video processing demands over 30 FPS inference, yet even the lightest published polyp-segmentation networks still carry 1 M parameters and must run on a GPU. This severely restricts deployment in primary hospitals, mobile devices, or embedded endoscopic systems [7, 26, 32]. Shrinking a model to a CPU-friendly size while preserving clinically usable accuracy, therefore, remains an open problem.

Current lightweight-colonoscopy research almost universally follows a “top-down” paradigm: start with a ResNet or ViT backbone pretrained on ImageNet, plug it into a U-shaped decoder to obtain a U-Net-like segmenter, and then compress further via pruning, structural re-design, or knowledge-distillation [5, 9, 22]. Yet, even under these performance-preserving constraints, the parameter count can only be pushed down to 1 M—still an order of magnitude too heavy for real-time CPU inference—leaving clinical roll-out “just out of reach”.

We observe that, in dermoscopy image analysis, the task is relatively well-defined, data quality is high, and sufficiently large annotated segmentation datasets are available. This has fostered several native ultra-light architectures—e.g., EGE-UNet and LB-UNet—with total parameters below 100 K [29, 41]. More importantly, dermoscopy and colonoscopy both image surface mucosal tissue, sharing similar low-level visual spaces in texture, color distribution, and lesion-boundary morphology. This finding opens a timely opportunity: instead of compressing a heavy network downward, can we start from a dermoscopy-validated “micro-backbone” and, through colonoscopy-oriented cross-modal structural re-design and adaptive enhancement, break the current 1 M parameter floor?

Guided by this insight, we establish a radically different “bottom-up” paradigm. We take a proven dermoscopic lightweight model as the seed, eschew traditional compression, and introduce (i) a cross-modal structural adapter and (ii) a colonoscopy-aware feature-enhancement module. Every architectural increment is governed by a strict “parametric minimalism” principle: any gain in segmentation performance must be purchased with the smallest possible parameter overhead. In this way, we trade upward only what is essential, achieving a precise equilibrium between capability and deployability.

We present UltraSeg, where ‘Ultra’ denotes the ultralight regime (< 0.3 M parameters), establishing the first strong baseline for CPU-real-time medical imaging. A family of ultra-lightweight networks tailored for real-time colonoscopic segmentation. Two instantiations are re-

leased: UltraSeg-108K, whose parameter count is squeezed to only 108 K, delivers over 90 FPS on a single CPU core and is intended for single-center, single-modality scenarios; and UltraSeg-130K, which augments the backbone with cross-layer attention and, at 130 K parameters, is optimized for multi-center, multi-modal training.

The models were evaluated on four public polyp-segmentation sets (CVC-ClinicDB, Kvasir, PolypGen, PolypDB) and one surgical-instrument set (Kvasir-Instrument). PolypDB blends five imaging modalities and PolypGen gathers data from six centers, jointly offering a rigorous generalization test. All experiments follow a strict intra-dataset 8:2 split. UltraSeg-108K achieves an average Dice of 0.7838 across the five colonoscopy sets, while UltraSeg-130K reaches 0.7926. Under the “extreme-compression” regime of < 0.3 M parameters (see below), our networks substantially outperform all existing peers, attaining 94 % of the accuracy of a 31 M-parameter U-Net while using only $\sim 0.4\%$ of its weights. Additional knowledge-distillation tests further reveal the limitations of conventional compression in this ultra-low-parameter regime. This work demonstrates that foresighted architectural design, rather than post-hoc compression, can yield high-performance AI ready for extremely resource-constrained environments.

¹

Operating well below this ceiling, the UltraSeg family exceeds 90 FPS on a single core, establishing the current best-performing lightweight solution for real-time colonoscopic video analysis on CPU-only hardware.

To summarize, our main contributions in this work are as follows:

1. We introduce a bottom-up paradigm for developing lightweight segmentation models, pushing single-core CPU inference beyond 90 FPS for the first time under a 0.3 M parameter budget and delivering a deployable real-time solution for primary hospitals and embedded endoscopic systems.
2. Starting from a lightweight backbone, we redesign the architecture for colonoscopic scenes and equip it with a progressive Enhanced-Dilated Block, markedly improving segmentation accuracy without sacrificing model compactness.
3. To counter inter-center and inter-modal variations, we propose a cross-layer attention-guided network that enhances generalization under complex conditions while adding negligible parameters.

¹We define the “extreme-compression” paradigm as models with < 0.3 M parameters, a threshold derived from the requirement of real-time (> 30 FPS) video inference on a commodity single-core CPU. Empirically, UNet-Small (0.389 M) runs at 41 FPS, whereas UNet-Light (0.861 M) drops to 24 FPS, confirming that extremely low parameter counts are crucial for CPU-side real-time operation.

2. Related Work

2.1. Medical Image Segmentation Model

The rise of convolutional neural networks (CNNs) has radically reshaped medical image segmentation. Among them, U-Net—with its encoder–decoder symmetry and skip connections—has become the *de facto* standard for a wide range of biomedical tasks [28]. Numerous successors enrich this backbone with attention mechanisms [29, 41], more elaborate decoders, or multi-scale feature fusion [9, 25], yielding steady gains on specific datasets.

Recently, Transformer architectures have been transplanted into medicine thanks to their capacity for global-context modeling [9, 22]. Swin-Transformer and pyramid vision transformers, for example, excel at capturing multi-scale spatial dependencies [23, 35, 36]. Meanwhile, state-space models such as Mamba are gaining traction for long-range dependency extraction, setting new performance records on several medical benchmarks [13, 37, 39].

However, a critical drawback accompanies this relentless pursuit of accuracy: model complexity and parameter count escalate sharply. Whether they are U-Net variants embellished with sophisticated modules or modern Transformer- and Mamba-based architectures, the number of trainable parameters easily reaches several tens or even hundreds of millions.

Meanwhile, the conspicuous domain gap between natural and medical images has fuelled a parallel trend—collecting millions of unlabeled images to pre-train domain-specific, self-supervised backbones. Such endeavours have proliferated across X-ray, fundus, pathology and colonoscopy imaging [18, 21, 34, 40]. Typically, a ResNet or Vision Transformer is first pre-trained with contrastive or masked-image modelling, then decapitated and appended with an upsampling decoder to form a segmentation network, before being fine-tuned on public benchmarks. In colonoscopy segmentation, this pipeline consistently outperforms its non-pre-trained counterparts. Yet, the ResNet-50 encoder alone carries 25 M parameters; coupled with a decoder, the overall model balloons to roughly 80 M in our measurements [18].

More recently, promptable segmentation models such as SAM have demonstrated mask-generation capabilities without task-specific annotations, offering a new paradigm for medical image analysis. Nevertheless, their clinical adoption remains tentative: the sheer model size hampers deployment, inference is computationally expensive, and their stability and accuracy on dedicated lesion segmentation tasks still lag behind specially trained lightweight networks [38].

In summary, although contemporary approaches have matured in accuracy and continue to set new performance records, they share a common deployment bottleneck. The

performance gains conferred by ever-larger architectures and self-supervised pre-training are approaching saturation, while the resulting model bulk renders GPU acceleration almost mandatory for real-time inference. This contradiction severely restricts the penetration of state-of-the-art algorithms into resource-constrained environments such as primary hospitals, mobile terminals, and embedded endoscopic systems, and represents the foremost obstacle to translating research breakthroughs into routine clinical practice.

2.2. Design of Lightweight Colonoscopy Segmentation Model

In the quest for lightweight colonoscopic segmentation, a growing body of work has sought a pragmatic balance between model size and accuracy. Polyp-PVT was the first to import Pyramid Vision Transformer weights pre-trained on natural images into polyp segmentation; by leveraging multi-scale global features, it achieved SOTA results in 2022 and firmly established the ViT family in this domain [9, 35]. Building on this, Polyp-LVT adopted a lightweight ViT backbone, integrated a scale-fusion module and a refined loss, and attained superior segmentation at a smaller footprint [22]. Another study refined DeepLabV3+ by coupling it with MobileNetV3 and retuning the ASPP dilation rates from 12-24-36 to 8-22-36 to better match polyp morphology, yielding a 6.18 M-parameter model [14]. LGPS, furthermore, proposed a lightweight GAN-based framework that compresses the total parameter count to 1 M [32].

Nevertheless, these efforts expose a shared limitation of current lightweight research: compression targets are typically set to the medium scale of 1–10 M parameters. Although this is already an order of magnitude smaller than the dozens-of-M baselines, it is still insufficient for fluent real-time inference on commodity CPUs, so the bottleneck to ubiquitous deployment remains intact. Colonoscopic or capsule-colonoscopic systems must therefore be paired with GPU servers to realize real-time video-based polyp detection.

An inescapable observation is that, with the advance of self-supervised learning and the collection of large-scale in-domain endoscopic images, simply taking a ResNet or ViT encoder pretrained on massive datasets and appending an upsampling head often outperforms most carefully crafted specialized architectures [18, 34]. This compels us to recalibrate the central mission of lightweight research: now that the path to “higher accuracy” is clear, we should instead ask, “When parameters are strictly rationed for CPU-side real-time segmentation, where is the fundamental performance floor?”

Motivated by the above, we recast lightweight polyp-segmentation research into two distinct paradigms:

- **Accuracy-first lightweight:** parameter budget is relaxed (e.g., > 1 M) and the goal is to approach or surpass the accuracy of large-scale models;
- **Extreme-compression lightweight:** parameters are strictly capped (e.g., < 0.3 M) to meet real-time, CPU-only video processing, seeking the optimal accuracy-efficiency trade-off and establishing a performance baseline for severely resource-limited scenarios.

Most existing studies follow the first paradigm, leaving the second largely unexplored. To fill this gap, we propose an ultra-lightweight model with fewer than 0.13 M parameters. Rather than competing with architectures an order of magnitude larger, our core contribution is to **establish, for the first time, a strong performance baseline under the extreme-compression paradigm**: our model achieves $> 94\%$ of the Dice score of a 31 M-parameter U-Net baseline while using only ~ 0.13 M parameters. This work demonstrates that high-quality AI can still be deployed in extremely resource-constrained environments and provides a reference for future ultra-lightweight research.

3. Method

To achieve high-accuracy yet ultra-efficient polyp segmentation in colonoscopy, we explore a bottom-up, extremely lightweight route. Reasoning that dermoscopy—like colonoscopy images surface mucosal tissue, we hypothesize that its state-of-the-art compact architectures can serve as a potent starting point. We therefore systematically evaluated two representative dermoscopic models, EGE-UNet and LB-UNet [29, 41]. Both build on an ultra-slim U-shaped CNN, inject deep supervision, and incorporate Hadamard-product-based linear attention, remaining below 0.1 M parameters while delivering strong results on public dermoscopy benchmarks. LB-UNet—equipped with dual-region and boundary supervision and a group-shuffle attention block—exhibits superior boundary awareness and discriminative power on colonoscopic data and was consequently adopted as our initial backbone.

However, the colonoscopic lumen is far more complex than skin surfaces: varying modalities, multi-center data, and indistinct polyp boundaries demand richer representations. The original LB-UNet suffers from a limited receptive field and insufficient cross-domain robustness, making it ill-suited for these challenges. We hypothesized that structural refinements with modest parameter increases could significantly boost colonoscopic segmentation performance.

To this end, we performed a series of colonoscopy-oriented architectural re-designs on LB-UNet at a restrained parameter cost, systematically enhancing multi-scale perception and cross-center generalization. The result is

an ultra-lightweight segmentation network, UltraSeg-108K, with merely 108K parameters, together with its multi-center, multi-modal extension, UltraSeg-130K. Figure 1 illustrates the overall framework of UltraSeg-130K; the following subsections elaborate on the design rationale and implementation details of each module.

3.1. Architectural Refinements

LB-UNet was originally tailored for dermoscopy and adopts the channel schedule [8, 16, 24, 32, 48, 64], which keeps many shallow-detail features. Colonoscopic frames, however, contain cluttered backgrounds, highly variable polyp shapes, and blurred boundaries; hence, stronger deep-semantics extraction is required.

We therefore reshape the channel list to [8, 16, 48, 64, 96]. By removing one downsampling stage and simultaneously expanding mid-/high-level channels, we obtain two key benefits: (i) the effective receptive field is enlarged, allowing the network to integrate broader contextual cues to detect polyps that visually merge with the mucosa; (ii) the discriminative power of deep features is strengthened, improving encoding of subtle morphological differences along indistinct polyp borders.

Regarding supervisory signals, LB-UNet iteratively generates boundary ground truth with a genetic algorithm—an expensive and opaque procedure. We replace it with a standard Canny edge detector (5×5 structural kernel). The new pipeline shortens boundary-label generation from hours to seconds, is fully deterministic and interpretable, and yields no degradation in segmentation accuracy.

Finally, we redesigned the predictive feature-fusion module. The original version fuses region and boundary predictions through manually tuned, fixed hyperparameters, offering no adaptability. We propose the Predict-Gated Fusion module, whose core innovation is a learnable weight vector coupled with a lightweight feature adaptor. The fusion process is formulated as:

$$\mathbf{x}_{\text{out}} = \mathbf{x}'_1 + \mathbf{x}_2 + \alpha \cdot \sigma(\mathbf{P}_{\text{region}}) \odot \mathbf{x}_2 + \beta \cdot \mathbf{P}_{\text{boundary}} \odot \mathbf{x}_2 \quad (1)$$

where \mathbf{x}'_1 denotes the decoder feature calibrated by the lightweight adaptor, \mathbf{x}_2 is the encoder feature delivered by the skip connection, $\sigma(\cdot)$ the Sigmoid function, $\mathbf{P}_{\text{region}}$ and $\mathbf{P}_{\text{boundary}}$ the region and boundary probability maps, and \odot the Hadamard product. Learnable scalar weights α (region_weight) and β (boundary_weight) replace the previously hand-tuned coefficients, enabling the fusion strategy to adapt automatically to the data distribution. This not only strengthens the model’s capacity to capture the complex appearances of colonoscopic polyps but also eliminates the uncertainty inherent in manual hyper-parameter tuning.

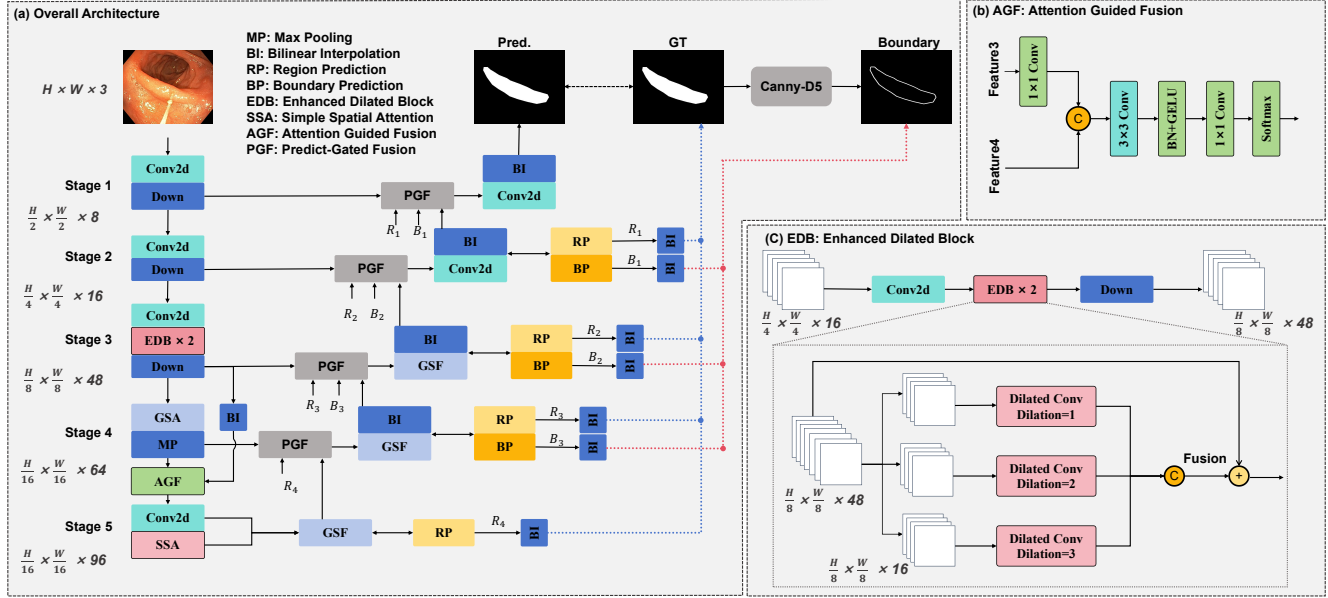


Figure 1. The architecture of our proposed methods.

Moreover, we retain the GSA (Group-Shuffle Attention) module and the separate region and boundary prediction heads from the original LB-UNet.

3.2. Enhanced Dilated Block

In the encoder, shallow layers capture local details such as color and texture, whereas deep layers learn highly abstract semantics. The third encoder block (`encoder3`) sits exactly at the transition from local details to global semantics: its feature map retains sufficient spatial resolution while already possessing rich semantic depth, making it an ideal place to inject multi-scale context.

To this end, we design the *Enhanced Dilated Block* (EDB). The input channels are evenly split into three groups, each undergoing depth-wise convolution with dilation rates 1, 2, and 3 in parallel. This allows the layer to simultaneously gather local fine structures, medium-range context, and larger global cues. The three branches are concatenated and fused by a 1×1 convolution.

Let the input tensor be $\mathcal{X} \in \mathbb{R}^{C \times H \times W}$. The EDB implements the mapping

$$\text{EDB}(\mathcal{X}) = \text{PWConv}\left(\parallel_{i=1,2,3} \text{DWConv}_{d=i}(\mathcal{X}_i; k=3, g=C/3)\right) \quad (2)$$

where \parallel denotes channel-wise concatenation, \mathcal{X}_i is the i -th equal-split partition of \mathcal{X} , $\text{DWConv}_{d=i}$ is depth-wise

convolution with dilation rate i , and PWConv is a 1×1 convolution for fusion.

For $C = 48$, two cascaded EDBs introduce 50k parameters, yet FLOPs drop by 0.04 G compared with the same-stage vanilla bottleneck (see Table 5), verifying that grouped dilated convolutions enlarge the receptive field without inflating computation.

Two cascaded blocks give a theoretical RF radius:

$$\text{RF} = 1 + 2(k-1) \sum_{i=1}^3 d_i = 13 \text{ pixels}, \quad (3)$$

equivalent to $13 \times 4 = 52$ pixels on the input image.

equivalent to $13 \times 4 = 52$ pixels on the input image (encoder3 stride 4), covering a ~ 50 -pixel diameter neighbourhood.

In other words, the network can dynamically integrate multi-scale information within a 50-pixel diameter neighbourhood—mimicking the human ability to reason “from a spot to a patch.” This progressive perception provides the spatial context essential for delineating blurred polyp boundaries and for distinguishing lesions from the complex intestinal background.

Inside each EDB, the 48 input channels are evenly split into 3 branches (16 channels each); every branch undergoes depth-wise dilated convolution, so each filter acts on exactly one channel, imposing structured sparsity and intra-group competition.

3.3. Cross-Layer Lightweight Fusion

Improving generalization across multi-center and multi-modal colonoscopy images usually relies on stacking channels or heavy self-attention—both violate our “parametric minimalism” principle. We therefore co-design two ultra-light modules: (i) **Attention-Guided Fusion (AGF)** that cross-fuses Stage-3 and Stage-4 features, and (ii) **Simple Spatial Attention (SSA)** that globally filters a $96 \times 16 \times 16$ bottleneck tensor without extra channels.

AGF (Fig. 1) first upsamples Stage-3 to $64 \times 16 \times 16$ via 1×1 conv, concatenates it with Stage-4 ($128 \times 16 \times 16$), then applies 3×3 conv \rightarrow BN \rightarrow GELU \rightarrow 1×1 conv. A Softmax produces two spatial masks α, β ($1 \times 16 \times 16$, $\alpha + \beta = 1$ pixel-wise). The final fused feature is $\alpha \odot \text{Stage-3}' + \beta \odot \text{Stage-4}'$ ($64 \times 16 \times 16$).

SSA averages AGF’s output along the channel axis, applies Sigmoid to obtain a $1 \times 16 \times 16$ gate, and re-weights the original feature with a learnable residual scalar α (initialised to 0.3):

$$\mathbf{x} = (1 - \alpha) \cdot \mathbf{x}_{\text{orig}} + \alpha \cdot \mathbf{x}_{\text{att.}} \quad (4)$$

This retains global context while suppressing redundant responses; α converges automatically during training. The whole attention suite consistently boosts segmentation generalisation across centers and modalities, requires no explicit label correction, and adds negligible overhead, fully satisfying the stringent resource budget of CPU-side real-time inference.

3.4. Loss Function

To fully exploit deep supervision and strengthen boundary awareness, we adopt a dual-task loss that simultaneously supervises region and edge predictions. The total loss is

$$\mathcal{L}_{\text{total}} = \mathcal{L}_{\text{region}} + \mathcal{L}_{\text{boundary}} + \mathcal{L}_{\text{gt}} \quad (5)$$

where

- $\mathcal{L}_{\text{region}}$ is the final region-segmentation loss computed as the BceDiceLoss (binary cross-entropy + Dice).
- $\mathcal{L}_{\text{boundary}}$ deep-supervises boundary predictions at three decoder levels with weights increasing with depth (0.1, 0.2, 0.3).
- \mathcal{L}_{gt} deep-supervises intermediate region predictions at four decoder levels with weights (0.1, 0.2, 0.3, 0.4).

3.5. Knowledge-Distillation Exploration

To probe further performance gains for an extremely small model, we experimented with feature-based knowledge distillation [27]. A 31 M-parameter U-Net served as

the teacher and UltraSeg as the student. The distillation loss is

$$\mathcal{L}_{\text{KD}} = \alpha \cdot \text{MSE}(\phi_t(\mathbf{x}), \phi_s(\mathbf{x})), \quad (6)$$

where ϕ_t and ϕ_s denote intermediate features of the teacher and student, respectively, and α is a balancing weight. We tested \mathcal{L}_{KD} at 10 %, 20 %, and 30 % of the original loss, each repeated three times, but observed no consistent improvement under the extreme-compression regime. We attribute this failure to:

1. **Capacity gap:** the student is $> 280 \times$ smaller, so its representation space is too impoverished to mimic the teacher’s high-dimensional features.
2. **Objective conflict:** the student is already heavily regularised by region-boundary dual supervision; the extra distillation term interferes with optimisation and prevents convergence to a better equilibrium.

This exploratory study demonstrates that conventional large-to-small distillation collapses when parameter ratios reach several orders of magnitude. Future work should investigate same-scale distillation or progressive-growth strategies better suited to extreme compression.

4. Experiments and Results

4.1. Baseline Models and Experimental Setup

To systematically evaluate the performance of the proposed model, this study compares it with three categories of representative baseline models: (1) The standard U-Net series serves as performance upper-bound references. We constructed four variants at different scales²: **UNet-Base**, **UNet-Medium**, **UNet-Light**, **UNet-Small**, and **UNet-Tiny**, forming a model spectrum with parameters ranging from 31M to 0.1M; (2) Lightweight general-purpose models (**FastSCNN**, **MobileUNet**), used to assess model compression efficiency; (3) Advanced lightweight models (**LB-UNet** and **EGE-UNet**), both improved based on the U-Net-Tiny architecture and validated effective in dermatoscopic segmentation tasks.

A detailed comparison of the number of parameters (Params), floating-point operations (FLOPs), and checkpoint sizes between all compared models and the proposed UltraSeg-108K series is presented in Table 1.

All experiments in this study were conducted on a single NVIDIA 5090 GPU under the PyTorch framework. To ensure robustness, each experiment was run three times with three fixed random seeds, and the mean and standard deviation are reported. The experimental settings were unified as follows: input image resolution 256 \times 256, batch size 4,

²U-Net channel configurations: Base: [64,128,256,512,1024]; Medium: [32,64,128,256,512]; Light: [24,48,96,192,384]; Small: [16,32,64,128,256]; Tiny: [8,16,32,64,128].

Table 1. Model complexity comparison.

Models	Params (M)	FLOPs (G)	Checkpoint Size (MB)
LB-UNet	0.038	0.098	0.3
EGE-UNet	0.053	0.072	0.4
UNet-Tiny	0.102	0.290	0.5
UltraSeg-108K	0.108	0.144	0.6
UltraSeg-130K	0.130	0.149	0.6
MobileUNet	0.140	0.170	0.6
FastSCNN	0.367	2.210	1.5
UNet-Small	0.389	1.007	1.6
UNet-Light	0.861	2.151	3.5
UNet-Medium	1.519	3.723	5.9
UNet-Base	31.0	54.8	119.0

number of data-loading workers 2; the optimizer was Adam with a learning rate of 3e-4; training lasted 100 epochs, and early stopping was triggered if the validation Dice coefficient did not improve for 10 consecutive epochs. Detailed model dimensions and channel designs are provided in our open-source GitHub repository and supplementary files.

4.2. Datasets and Evaluation Metrics

The experiments in this study were conducted on four authoritative polyp segmentation datasets: CVC-ClinicDB [4], Kvasir-SEG [16], PolypGen [2], and PolypDB [17]. Among them, CVC-ClinicDB and Kvasir-SEG consist of data collected from a single institution and a single imaging device. In contrast, the PolypGen dataset aggregates images from six different medical centers. At the same time, PolypDB is even more complex, containing five different imaging modalities (BLI, FICE, LCI, NBI, WLI) from three distinct centers.

To assess the model’s general-purpose segmentation capability under colonoscopic imaging conditions, we additionally evaluated it on the Kvasir-Instrument dataset [15], a surgical-tool segmentation benchmark. In this setting, the task is no longer polyp delineation, but the comparatively simpler detection of GI-procedure instruments—snares, balloons, biopsy forceps, etc.

Furthermore, we conducted external validation on two completely unseen datasets, ETIS-Larib [11] and BKAI-IGH [31], both providing expert pixel-level gold standard masks for 196 and 1,000 colonoscopy images, respectively.

As all datasets consist of independent static frames rather than continuous video sequences, we follow the standard evaluation protocol of image segmentation and randomly split each dataset into 80% for training and 20% for testing. This guarantees that the model is assessed on unseen but distributionally consistent samples, providing an unbiased estimate of its generalization ability and avoiding performance inflation due to inter-frame correlation.

It should be emphasized that the naturally imbalanced multi-center and multi-modal distribution persists in both the training and test subsets of PolypGen and PolypDB. For instance, the least-represented modality in PolypDB contains only 60 images, whereas the most-represented one comprises 3,588 images. Such severe skew poses a formidable challenge for learning and generalization, yet it also renders the evaluation results more clinically relevant.

Table 2 details the characteristics of this study. Please refer to the supplementary document for the detailed training set, test set data, and multi-center multimodal partitioning details.

In this study, the Dice coefficient is employed as the primary evaluation metric for all experiments, with IoU and 95th percentile Hausdorff Distance (HD95, in pixels) additionally reported. The corresponding formulas are given below:

$$\text{Dice} = \frac{2|X \cap Y|}{|X| + |Y|} = \frac{2\text{TP}}{2\text{TP} + \text{FP} + \text{FN}} \quad (7)$$

$$\text{IoU} = \frac{|X \cap Y|}{|X \cup Y|} = \frac{\text{TP}}{\text{TP} + \text{FP} + \text{FN}} \quad (8)$$

$$\text{HD95} = P_{95} \left(\left\{ \min_{y \in Y} d(x, y) \right\}_{x \in X} \cup \left\{ \min_{x \in X} d(x, y) \right\}_{y \in Y} \right) \quad (9)$$

where X and Y denote the predicted and ground truth segmentation masks, respectively; TP, FP, FN represent true positives, false positives, and false negatives; $d(\cdot, \cdot)$ denotes the Euclidean distance, and P_{95} denotes the 95th percentile. Notably, Dice and IoU measure region overlap, where higher values indicate better segmentation accuracy. Conversely, HD95 quantifies boundary discrepancy, where lower values signify superior boundary alignment and reduced outlier sensitivity.

Table 2. Overview of datasets in this study

Dataset	Data Source	Task	Num. of Images	Usage
CVC	Single-center, single-device	Polyp segmentation	612	Development
Kvasir	Single-center, single-device	Polyp segmentation	1,000	Development
Kvasir-Inst	Single-center, single-device	Instrument segmentation	590	Development
PolypGen	Multi-center (6 institutions)	Polyp segmentation	1,537	Development
PolypDB	Multi-modalities (5 modalities)	Polyp segmentation	3,934	Development
ETIS-Larib	Single-center, single-device	Polyp segmentation	196	External validation
BKAI-IGH	Single-center, single-device	Polyp segmentation	1,000	External validation

Note: CVC = CVC-ClinicDB; Kvasir = Kvasir-SEG; Kvasir-Inst = Kvasir-Instrument. Datasets marked as "Development" were used for model training and internal validation, while "External validation" datasets were used solely for independent testing.

4.3. Main Results

We initially restrict development and testing to a single-center database. Table 3 summarizes our main results. All models were run three times under a fixed random seed; the table reports the mean scores. As shown, our method achieves a clear margin over competing models with fewer than 0.3 M parameters on all five colonoscopic segmentation tasks.

In the four colonoscopic polyp segmentation tasks, CVC and Kvasir are regarded as relatively "easy" benchmarks because they are single-modality and single-center datasets. On CVC, the 31M parameter UNet-Base achieves 0.9099 Dice, whereas the 1.519M parameter UNet-Medium only reaches 0.8356. Our baseline model, with merely 0.108M parameters, obtains 0.8475 Dice and 0.7428 IoU, outperforming all lightweight competitors under 0.3M parameters and even surpassing UNet-Medium. The same trend is observed on Kvasir: our model ranks first with 0.7516 Dice, significantly ahead of the best lightweight counterpart and still exceeds UNet-Medium, whose parameter count is 14 \times larger.

On the multi-modal, multi-center PolypDB dataset, the proposed method attains 0.7697 Dice. Among existing lightweight models, the highest performance is delivered by LB-UNet, a dermoscopy segmentation network that is fully transferred to colonoscopy (0.7411 Dice). EGE-UNet, another lightweight architecture equipped with deep supervision, only reaches 0.6338 Dice, while the standard lightweight MobileUNet drops to 0.3408 Dice, markedly lower than our result.

On the multi-center polyp segmentation dataset PolypGen, the proposed method achieves 0.6496 Dice, which remains markedly superior to all lightweight models of comparable size and approaches the performance of UNet-Medium. Experimental analyses reveal that PolypGen exhibits pronounced inter-center variations; under the con-

straints of ± 1 M parameters, absence of pretrained backbones, and limited training samples, lightweight architectures struggle to learn robust representations, resulting in widespread performance degradation.

The enhanced UltraSeg-130K, specifically designed for multi-center and multi-modal data, incurs only a marginal decrease in single-center sets such as CVC and Kvasir relative to UltraSeg-108K. However, its advantages become pronounced in cross-center and cross-modal scenarios: average Dice on PolypDB rises to 0.7820, and on PolypGen reaches 0.6826, both significantly exceeding UNet-Medium and representing substantial gains over the baseline UltraSeg-108K.

As a control experiment, the Kvasir-Instrument dataset—created for surgical-instrument segmentation in colonoscopy—presents a distinctly easier task. Instruments exhibit much higher contrast against the intestinal wall than polyps, and their boundaries are sharply defined. Both proposed models set a new state of the art on this dataset, attaining Dice scores of 0.9006 and 0.9065, respectively. These results surpass not only the strong lightweight baselines LB-UNet and FasterSCNN, but also the full-capacity UNet baseline with substantially more parameters.

Across the five colonoscopic segmentation sets, each with distinct visual characteristics, we observe a clear trend for plain UNet variants: without any architectural refinement, the average Dice monotonically decreases as the parameter count is reduced solely by shrinking channel widths. UNet-Base, whose capacity is roughly 20 \times that of UNet-Medium, delivers an average 0.056 Dice points higher, confirming that increased model capacity alone can yield meaningful gains even in the absence of structural redesign.

Overall, our solution achieves the highest mean Dice of 0.7926 across the five tasks, outperforming the strong reference LB-UNet by 0.046 and exceeding UNet-Medium, while achieving 94.49% of the performance of the 31M

Table 3. Main segmentation performance comparison. Our proposed UltraSeg-108K and UltraSeg-130K have achieved leading or highly competitive performance compared to other extremely lightweight models in polyp and instrument segmentation tasks under a colonoscopy background.

Models	PolypDB		PolypGen		CVC		Kvasir		Kvasir-Inst		Avg Dice↑
	Dice↑	IoU↑									
UNet-Base	0.8536	0.7586	0.7288	0.6157	0.9099	0.8385	0.8247	0.7128	0.8770	0.7899	0.8388
UNet-Medium	0.7776	0.6525	0.6757	0.5311	0.8356	0.7265	0.7424	0.5999	0.8796	0.7940	0.7822
UNet-Light	0.7765	0.6548	0.6660	0.5321	0.7975	0.6730	0.7385	0.5965	0.8884	0.8076	0.7734
UNet-Small	0.7525	0.6238	0.6056	0.4609	0.7770	0.6459	0.7076	0.5575	0.8771	0.7887	0.7440
UNet-Tiny	0.6683	0.5256	0.5431	0.3933	0.6485	0.4900	0.6146	0.4588	0.8167	0.7014	0.6583
FastSCNN	0.6355	0.4812	0.5813	0.4249	0.7945	0.6669	0.5827	0.4243	0.8988	0.8223	0.6986
MobileUNet	0.3408	0.2189	0.3725	0.2432	0.5635	0.4044	0.4652	0.3115	0.8316	0.7201	0.5147
EGE-UNet	0.6338	0.4778	0.5279	0.3719	0.5894	0.4264	0.6354	0.4765	0.8146	0.6976	0.6402
LB-UNet	0.7411	0.6066	0.6144	0.4632	0.7856	0.6575	0.6940	0.5422	0.8978	0.8184	0.7466
UltraSeg-108K	0.7697	0.6435	0.6496	0.5022	0.8475	0.7428	0.7516	0.6106	0.9006	0.8231	0.7838
UltraSeg-130K	0.7820	0.6560	0.6826	0.5380	0.8430	0.7358	0.7489	0.6077	0.9065	0.8325	0.7926

parameter UNet-Base. Notably, the proposed approach demonstrates particularly strong learning capability on relatively tractable tasks, as evidenced by its superior results on both CVC and Kvasir-Instrument datasets.

4.4. Comparison with Lightweight Baselines

Table 4 reports the average frames-per-second (FPS) and latency obtained by continuously inferring 1,000 images on CPUs. The Average Dice column summarizes the mean Dice score across five public datasets. The 24-Core test exploits all cores of an Intel i9-14900K, whereas the Single-Core test is restricted to one core to emulate resource-limited edge scenarios.

Under single-core conditions, our model attains 90.3 FPS, on par with extremely lightweight competitors such as LB-UNet and EGE-UNet, and markedly outperforms the 31M parameter UNet-Base.

UNet-Light (0.861 M parameters) achieves 24.6 FPS on one core, UNet-Small (0.389 M) reaches 41.6 FPS, while colonoscopy video is typically captured at 30 FPS. Consequently, for low-cost real-time segmentation on a CPU, the parameter budget should be kept below 0.4M, and preferably under 0.3M.

Coupled with the main results, our model delivers the highest average Dice while maintaining top-tier inference speed, offering a clearly better precision-efficiency trade-off than fast but inaccurate alternatives such as MobileUNet.

Figure 2 presents scatter plots of parameter count *vs.* Dice and single-core CPU-FPS *vs.* Dice for all models except UNet-Base. The red five-pointed star denotes our proposed UltraSeg family. Compared with specialized lightweight models under 0.3M parameters and with various UNet variants alike, UltraSeg achieves the highest Dice while maintaining an extremely small footprint and deliv-

ering over 90FPS on a single CPU core, fully meeting the demands of real-time inference on edge devices. Our proposed solution maintains both parameter count and FPS at highly competitive levels while achieving superior accuracy, realizing the optimal balance between precision and speed.

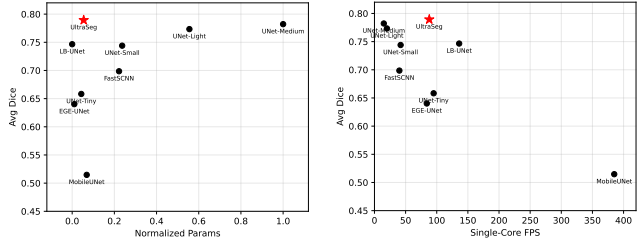


Figure 2. Left: Params-Dice trade-off; Right: Single-core FPS-Dice trade-off. Our UltraSeg-Family (red star) simultaneously achieves the best accuracy and superior efficiency.

4.5. Visualization and Qualitative Analysis

Figure 3 compares segmentation results on representative test images among UNet-Tiny, the strongly supervised baseline LB-UNet, and our proposed UltraSeg-108K/130K. Regardless of polyp size or quantity, our proposed models consistently surpass competitors owing to fine-grained architectural refinements under an extreme parameter budget. Nevertheless, edges remain blurred for all tiny models. This is an inherent bottleneck arising from the interplay between limited capacity and scarce training data. Premature down-sampling in the encoder dilutes shallow edge cues, while decoders with limited channels cannot fully reconstruct high-resolution details, leading to jagged boundaries and incomplete or excessive segmentation. Notably, UltraSeg-

Table 4. Model performance comparison on CPU-based hardware platforms

Models	Avg Dice	24-Core Test		Single-Core Test	
		FPS	Latency(ms)	FPS	Latency(ms)
UNet-Base	0.8388	9.2	109.0	1.6	618.3
UNet-Medium	0.7822	47.1	21.2	13.8	72.5
UNet-Light	0.7734	73.6	13.6	24.6	40.6
UNet-Small	0.7440	88.3	11.3	41.6	24.1
UNet-Tiny	0.6583	126.4	7.9	95.6	10.5
FastSCNN	0.6986	168.9	5.9	40.0	25.0
MobileUNet	0.5147	720.8	1.4	385.3	2.6
EGE-UNet	0.6402	137.6	7.3	84.1	11.9
LB-UNet [†]	0.7466	73.1	13.0	109.7	9.1
UltraSeg-108K	0.7838	128.1	8.0	92.1	11.4
UltraSeg-130K	0.7926	128.8	8.0	90.3	11.1

[†] Negative scaling: single-core FPS 136.7 due to synchronization overhead.

130K best mitigates these jagged polyp edges within the constrained parameter budget, delivering substantially superior delineation.

Figure 4 compares the proposed method with the baselines UNet-Tiny and LB-UNet on PolypDB and PolypGen datasets. Building upon UltraSeg-108K, UltraSeg-130K introduces attention-guided skip connections after the 3rd and 4th downsampling stages and adds an extra spatial-attention residual block after the bottleneck.

Experiments show consistent gains in sample-level Dice and modality-averaged Dice. Our cross-layer attention fusion at the end of downsampling boosts the generalization of a lightweight model during multi-modal, multi-center training, without extra labels and with negligible extra parameters. The approach remains robust even when sample sizes are highly imbalanced across centers or modalities.

In summary, this strategy effectively mitigates distribution shift with only a small increase in parameters, ensuring stable segmentation performance across institutions and devices and thus facilitating clinical deployment.

4.6. Ablation Experiments

Table 5 systematically presents the step-wise improvements and ablation analysis on the lightweight baseline UNet-Tiny and the stronger LB-UNet. All results are averaged over three independent runs to ensure robustness.

First, LB-UNet significantly boosts performance over UNet-Tiny by introducing joint deep supervision for both region and boundary, yielding consistent gains across all five colonoscopy datasets and establishing a solid starting point for further enhancements.

Building upon this, we introduce task-specific architectural refinements (denoted as US-108K (ST)). Although parameter count increases from 38 K (LB-UNet) to 60 K, clear performance improvements are observed on every dataset, with a Dice gain of 0.0155 on the CVC set. These results demonstrate that the proposed adaptations better capture the characteristics of colonoscopic images while simplifying hyper-parameter tuning and reducing reliance on complex pre-processing such as genetic algorithms.

Subsequently, we inserted two progressively dilated layers after the third downsampling stage by introducing the Enhanced Dilated Block (EDB), yielding the US-108K (ST+EDB) variant. Parameter count rose to 108K, yet performance jumped markedly—Dice on the Kvasir set improved by 0.0361, a substantial gain for a sub-0.1M segmentation model.

Finally, our cross-layer, attention-guided module tailored for multi-center/multi-modal data delivered further, steady improvements on the pooled datasets at the cost of only a few thousand extra parameters, demonstrating that pronounced distributional gaps can be mitigated within an

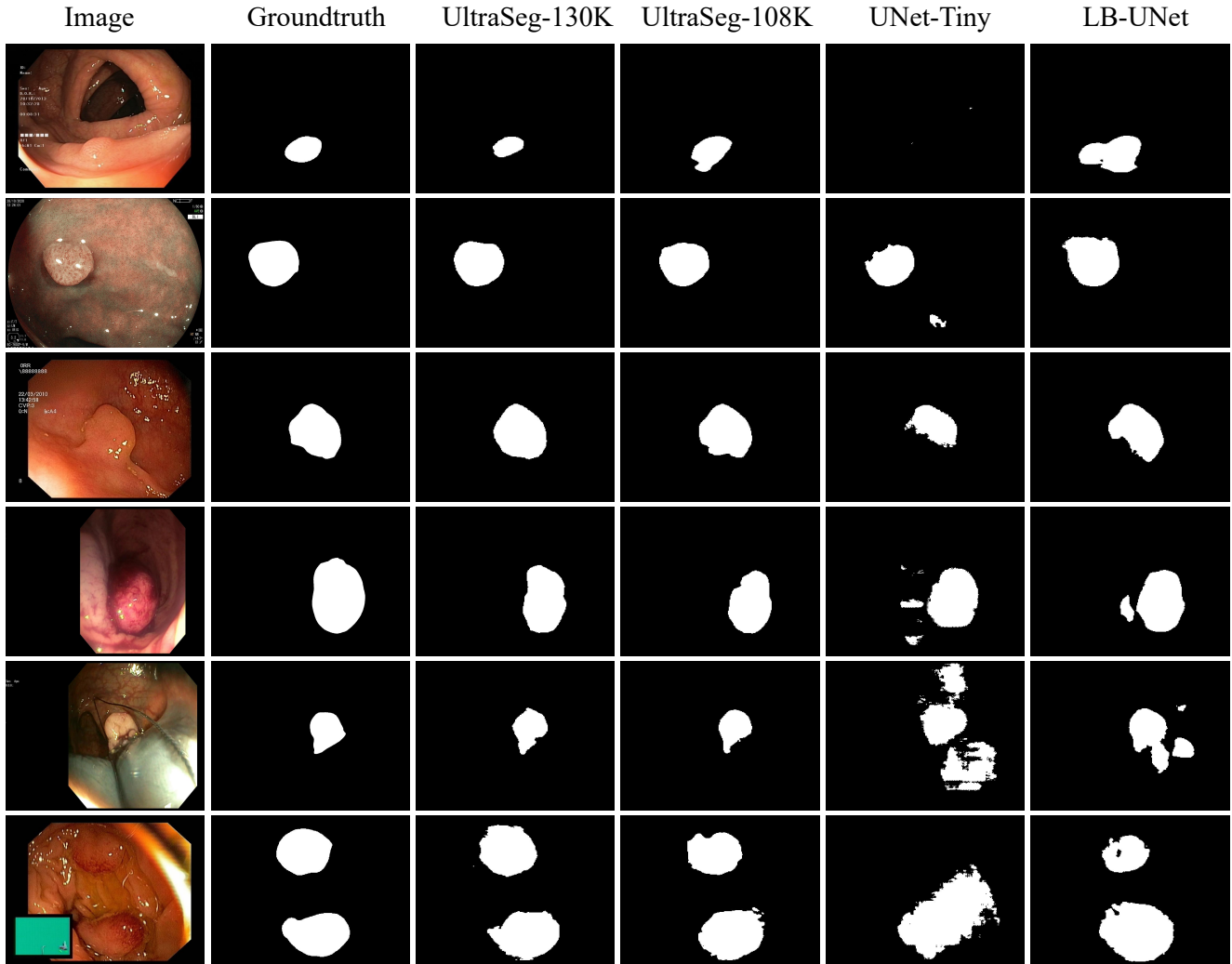


Figure 3. Qualitative comparisons on lightweight models.

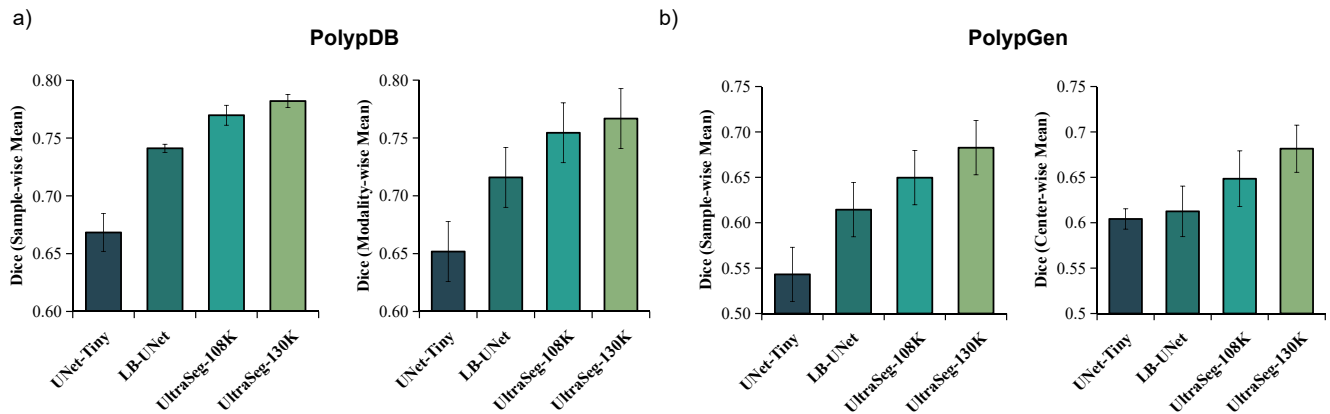


Figure 4. The figure presents the per-sample mean Dice and the center- or modality-level mean Dice for different models on the PolypDB and PolypGen datasets.

ultra-lightweight backbone. Throughout these ablations, we kept channel widths unchanged to maintain the desired model size. This bottom-up lightweight model construction scheme accurately switches parameter growth to Dice’s indicator growth at each step, and FLOPs do not significantly increase or even decrease, achieving SOTA lightweight within 0.15 G.

We note that publicly available, fully annotated multi-modal and multi-center colonoscopy datasets remain scarce, limiting broader validation on larger-scale heterogeneous data; expanding data sources is an important next step.

4.7. Extreme-compression Models Benefit More from Data Scaling

To verify whether extremely lightweight models can achieve better performance gains as the amount of gold-standard polyp datasets increases, we unified and merged four colonoscopic polyp segmentation datasets and split them into training and test sets at a ratio of 8:2. As shown in Table 6, when the four datasets are combined for training and testing, the proposed extremely lightweight solution still achieves the best performance among lightweight models, with further improvements in all metrics. Specifically, UltraSeg-108K reaches a Dice of 0.7884, while UltraSeg-130K attains a Dice of 0.8038 and an HD95 of 37.31 px. These results not only significantly outperform other lightweight models but also approach the performance of UNet-Medium. As the training dataset expands and multi-center, multi-modal data are included, although UNet-Base still achieves better performance relying on its parameter advantage, the gap between it and UNet-Medium, as well as our UltraSeg-130K, is further narrowed. UNet-Light, UNet-Medium, UltraSeg-130K, and UNet-Base all exceed 0.8 Dice, while our HD95 performance is only slightly behind that of UNet-Base, demonstrating a more sensitive perception of boundaries.

Furthermore, we conducted external validation on two completely unseen datasets, ETIS-Larib [11] and BKAI-IGH [31]. These independent cohorts enable an unbiased assessment of cross-domain generalization.

As shown in Table 6, UltraSeg-130K consistently outperforms UltraSeg-108K on both benchmarks, achieving the highest Dice coefficients of 0.6821 on ETIS-Larib and 0.8001 on BKAI-IGH. These scores narrow the gap with UNet-B to only 2.0 and 1.6 percentage points, respectively, while significantly exceeding UNet-M and other compact architectures. Despite requiring more than ten times fewer parameters than full-sized counterparts, our lightweight solution delivers accuracy previously reserved for heavyweight networks.

Crucially, the same model trained on the diversified mixed dataset markedly surpasses its counterpart trained on any single cohort, underscoring the strong capacity of Ultra-

Seg to exploit heterogeneous data and confirming that scale and variety in gold standard annotations are key to realizing real-time, CPU-friendly polyp segmentation without sacrificing accuracy.

4.8. Qualitative Analysis of Remaining Challenges

We highlight the challenges and typical failure cases of our proposed UltraSeg-130K lightweight model through inference results on the external datasets ETIS-Larib and BKAI-IGH using models trained on the merged dataset. Figure 5 displays representative failure cases alongside corresponding predictions from the 31M parameter UNet Base and ground truth masks. A consistent pattern emerges: when polyps are unusually large or appear as multiple scattered lesions, UltraSeg-130K reliably detects their presence but yields noticeably coarser boundary delineation. These imprecise contours on large or multi-polyp cases are the primary factor causing the lightweight model to lag behind UNet Base by several percentage points on both external benchmarks. Visualizing such systematic errors not only explains the remaining performance gap but also identifies targeted improvements for our next steps, whether through architectural adjustments, boundary-aware losses, or synthetic data augmentation.

4.9. Analysis on Knowledge Distillation

Although our 130K parameter model surpasses other lightweight rivals on all colonoscopy datasets, it still trails medium to large architectures such as the 31M parameter UNet Base. To extract further improvements without additional weights, we employed knowledge distillation from the stronger teacher.

We applied feature-based knowledge distillation on the relatively large PolypDB and PolypGen sets using loss weights of 10%, 20%, and 30%. The Feature KD Dice column shows the best result for each weight.

Experiments show that knowledge distillation yields only marginal gains for the UltraSeg family. We attribute this limitation to two interacting factors. First, the network already employs joint region-and-boundary deep supervision; the additional high-dimensional feature-matching objective conflicts with these fine-grained signals and diverts attention from task-specific cues. Second, at a compression ratio of 300:1, the 31 million-parameter teacher’s high-level embeddings surpass the expressive capacity of the 108 thousand-parameter student, so forcing the student to replicate unattainable representations is inefficient and can even be detrimental.

Without additional data, every model has an inherent performance saturation point. Under extreme parameter constraints and already elaborate supervision, classic feature knowledge distillation is unlikely to substantially break this ceiling for ultra-lightweight networks.

Table 5. Ablation study on the proposed architectural components.

Method	Params (M)	FLOPs (G)	PolypDB	PolypGen	CVC	Kvasir	Kvasir-Inst
UNet-Tiny ^a	0.102	0.290	0.6683 \pm 0.0163	0.4274 \pm 0.0246	0.6485 \pm 0.0521	0.6146 \pm 0.0443	0.8167 \pm 0.0356
LB-UNet ^b	0.038	0.072	0.7411 \pm 0.0035	0.6144 \pm 0.0091	0.7856 \pm 0.0109	0.6940 \pm 0.0071	0.8978 \pm 0.0072
UltraSeg-108K (ST) ^c	0.060	0.185	0.7447 \pm 0.0059	0.6300 \pm 0.0039	0.8011 \pm 0.0083	0.7155 \pm 0.0133	0.8990 \pm 0.0030
UltraSeg-108K (ST+EDB) ^d	0.108	0.144	0.7697 \pm 0.0086	0.6496 \pm 0.0153	0.8475 \pm 0.0132	0.7516 \pm 0.0037	0.9006 \pm 0.0030
UltraSeg-130K (ST+EDB+AGF+SSA) ^d	0.130	0.149	0.7820 \pm 0.0057	0.6826 \pm 0.0117	0.8430 \pm 0.0039	0.7489 \pm 0.0081	0.9065 \pm 0.0064

^a Vanilla lightweight baseline.^b Strong lightweight baseline from dermoscopy.^c **US-108K** with Structural Tweaks.^d (c) + Enhanced Dilated Convolution Blocks (2 \times at e3) (Ours).^e (d) + AGF, SSA modules provide cross-Layer Lightweight Fusion ability (Ours).

Table 6. Segmentation performance on Mixed dataset and inference results on two external datasets (mean of 3 runs with different seeds).

Model	Mixed Dataset			ETIS-Larib External			BKAI-IGH External		
	Dice \uparrow	IoU \uparrow	HD95 \downarrow	Dice \uparrow	IoU \uparrow	HD95 \downarrow	Dice \uparrow	IoU \uparrow	HD95 \downarrow
UNet-B	0.8478	0.7412	33.48	0.7094	0.5830	38.09	0.8163	0.7045	26.28
UNet-M	0.8131	0.7010	40.82	0.6295	0.4908	47.59	0.7764	0.6539	33.06
UNet-L	0.8034	0.6816	46.30	0.6234	0.4843	58.69	0.7697	0.6467	37.12
UNet-S	0.7704	0.6570	44.23	0.5826	0.4484	61.01	0.7337	0.6021	36.52
UNet-T	0.6716	0.5201	50.24	0.4602	0.3375	67.61	0.6097	0.4667	ina
FastSCNN	0.6685	0.5182	80.70	0.4686	0.3245	100.94	0.6209	0.4701	78.80
MobileUNet	0.4879	0.3229	93.49	0.2248	0.1346	102.39	0.4443	0.3013	94.29
EGE-UNet	0.7079	0.5632	59.22	0.5547	0.4118	66.34	0.6878	0.5438	51.04
LB-UNet	0.7685	0.6425	40.74	0.6437	0.5062	57.12	0.7700	0.6435	35.15
UltraSeg-108K	0.7884	0.6676	39.96	0.6736	0.5387	53.66	0.7873	0.6662	31.97
UltraSeg-130K	0.8038	0.6882	37.31	0.6821	0.5478	50.24	0.8001	0.6796	30.50

ina: HD95 omitted due to excessive calculation error.

5. Discussion

This study introduces the UltraSeg family: a 108 K-parameter lightweight model for single-center, single-modality polyp segmentation and a 130 K-parameter model for multi-center, multi-optical-modality colonoscopy scenes. Following a “minimal-parameter” principle, every additional module is designed to yield maximum performance gains across multiple datasets at the lowest possible parametric cost. The models achieve competitive results on seven public colonoscopy segmentation datasets, convincingly demonstrating that reliable pixel-level segmentation is attainable under extreme parameter constraints.

Currently, most lightweight polyp segmentation studies (such as Polyp-PVT, Polyp-LVT) follow the ‘accuracy first’ paradigm, with parameter budgets typically above 10M, and generally rely on pre-trained backbone networks on large-scale natural image datasets such as ImageNet [8, 22, 36]. Although this paradigm has achieved excellent accuracy

in computationally resource-rich environments, its model size and pre-training dependencies make it impossible to achieve real-time inference in pure CPU, resource-limited clinical scenarios. This study aims to explore a completely different paradigm of ‘extreme compression’, with the core constraint of strictly limiting the number of parameters to below 0.3M, training from scratch, and meeting real-time video processing requirements of over 30 FPS on a single CPU core. Under this paradigm, traditional lightweight methods based on pre-trained large models cannot be short-listed due to size and computational overhead. Therefore, the baseline for this work should be a model that is in the same ‘arena’ as ours: a network with fewer than 0.3M parameters, also not relying on external pre-training, and designed for CPU deployment (such as LB-UNet, MobileUNet, and FastSCNN). Our contribution lies in establishing a powerful performance benchmark for the first time in this previously unexplored field of ‘extreme compression’.

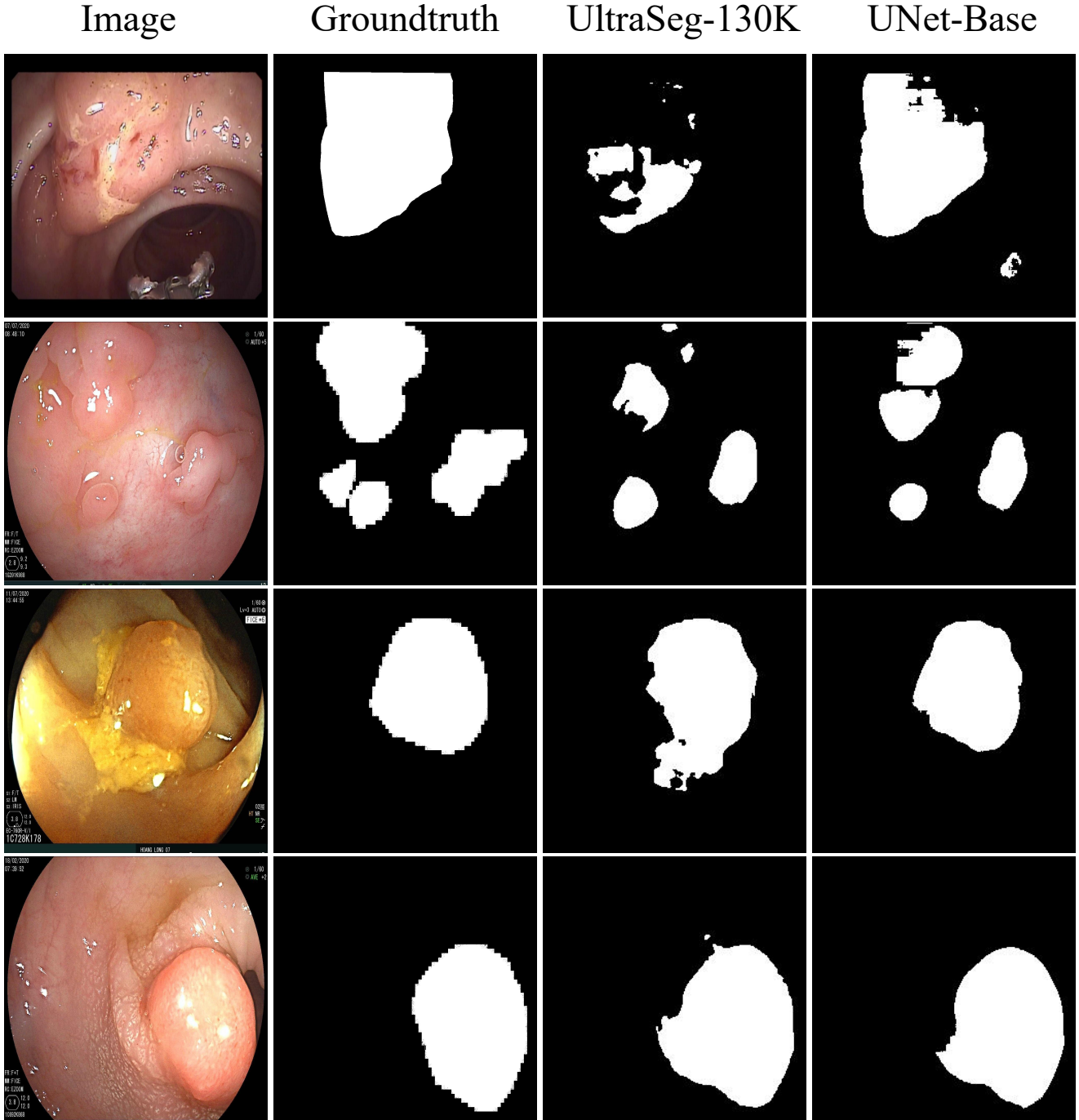


Figure 5. Typical cases of significant prediction errors in Ultraseg-130K.

This study proposes a lightweight path that contrasts with the mainstream "top-down" paradigm. Existing methods rely heavily on visual extractors pre-trained on large natural images, which use attention and multi-scale fusion to achieve high accuracy. However, this approach leads to a significant increase in parameter count and strong GPU dependence, which hinders its clinical imple-

mentation. We take advantage of the commonality between dermatoscopy and colonoscopy in terms of surface optical imaging, blurred lesion boundaries, and variable morphology. Starting from the validated ultra-light dermatoscopy skeleton, we only make structural adjustments for colonoscopy features to obtain an efficient segmentation model with 108 k/130 k parameters and CPU deploy-

Table 7. Performance Comparison of Feature-based Knowledge Distillation Across Datasets and Model Variants

Model Variant	Baseline Dice	Feature KD Dice	Δ Dice
PolypDB Dataset			
UltraSeg-108K	0.7697	0.7749	+0.0052
UltraSeg-130K	0.7820	0.7865	+0.0045
PolypGen Dataset			
UltraSeg-108K	0.6496	0.6619	+0.0123
UltraSeg-130K	0.6826	0.6812	-0.0014

ment, achieving "bottom-up" cross-domain migration. The core advantage of this method is that it does not passively prune redundant models but actively introduces efficient inductive biases that have been verified in similar visual tasks, thereby achieving steady performance improvements from an extremely low parameter starting point. The lightweight pathway revealed in this study stands in sharp contrast to the prevailing paradigm of "large model + complex modules." The latter aims to push the performance ceiling in compute-rich environments, whereas our work strives for practical breakthroughs under strictly limited resources. The two approaches are not ranked; they serve distinct clinical goals.

Compared with existing lightweight models whose parameters commonly exceed 1M, this study breaks new ground by pushing model complexity down an entire order of magnitude. Under fair and strictly enforced dataset splits, and constrained to real-time inference of $\lesssim 30$ FPS on a single CPU core, our model delivers the best performance reported to date, even though its absolute accuracy still trails large-scale counterparts. This usability leap carries greater practical weight for rolling out AI colonoscopy screening in primary-level or resource-limited settings than the few extra percentage points gained on GPU servers. The work demonstrates that, through judicious cross-domain architecture transfer and task-specific refinements, an extremely compressed model can remain clinically viable. We firmly believe that, for AI medical tools intended for wide deployment, breakthroughs in feasibility are as critical as pushing accuracy to its limits.

Despite the encouraging results achieved by the UltraSeg family, we are acutely aware that a performance gap remains compared with large-parameter models. We recognize that the order-of-magnitude difference in model capacity constitutes a natural and formidable upper bound—an inherent constraint that any "extreme compression" paradigm must accept.

The UltraSeg family demonstrates that high-quality segmentation is feasible under extreme compression. However, the pursuit of such efficiency inevitably encounters fundamental trade-offs. Firstly, the constrained capacity poses challenges in modeling highly heterogeneous data distri-

butions, such as those arising from multi-center or multi-modal imaging protocols. This is reflected in the performance gap of different models between the CVC dataset and the PolypGen dataset. Secondly, maintaining long-range spatial coherence for extensive lesions remains challenging within a sub-0.15M parameter budget, occasionally leading to fragmented predictions in large polyp cores. Thirdly, the same budget limits the fidelity of boundary cues, so edges are noisier and more ragged than those delivered by larger models.

To explore the limits of performance gains, we systematically experimented with knowledge distillation, aiming to transfer the rich representations extracted from UNet-Base into our lightweight model. However, experimental results showed that this approach failed to deliver the expected significant improvements. First, our model already integrates dual deep supervision over both regions and boundaries to achieve high accuracy, resulting in a complex composite loss function. The additional distillation loss term may introduce conflicts among different optimization objectives, thereby constraining the model's ultimate convergence potential. Second, and more fundamentally, there may be an intrinsic difference in the feature-representation learning mechanisms between the teacher model and the extremely lightweight student model; the complex, high-dimensional feature distribution learned by the teacher may exceed the structural representational capacity of the parameter-constrained student, rendering knowledge transfer ineffective.

This negative outcome offers deeper insights. Looking ahead, we believe that performance gains in extremely lightweight models can still be pursued along two complementary avenues:

First, model scaling within a controllable range. Under the hard constraint of maintaining real-time CPU inference ($\lesssim 30$ FPS), we moderately expand the model size to probe the performance ceiling. Preliminary experiments show that a parameter count of 300–400 K still satisfies the requirement of purely CPU-based real-time processing. We will therefore systematically study scaling laws, increase capacity by adding a modest number of parameters, and

build an UltraSeg family that covers diverse accuracy-speed trade-offs, flexibly fitting clinical scenarios from mobile endoscopy to standard workstations.

Second, design a pre-training paradigm tailored to ultra-light models. Recent work has demonstrated the benefit of self-supervised learning on colonoscopic images for downstream segmentation, yet these studies all rely on large backbones such as ResNet or ViT. A natural question is whether such gains can trickle down to extremely small networks. We argue that prevailing self-supervised objectives (e.g., MAE, contrastive learning) are strongly coupled to the capacity of large models. Hence, we will explore customized pre-training strategies dedicated to “extremely compressed” architectures, aiming to further boost the feature-extraction capability of lightweight models in the colonoscopy domain.

Thus, these challenges do not undermine the viability of the extreme-compression paradigm, but rather define its evolving research frontier. The UltraSeg family establishes the baseline from which this exploration can proceed. The experimental results in this paper give us strong confidence. Provided there is a sufficient volume of diverse, multi-center, multi-modal labeled data for training, our model has the potential to deliver real-time, accurate lesion segmentation on pure CPU platforms, offering a practical technical route to drastically lower the clinical-deployment barrier for AI-assisted colonoscopy screening.

6. Conclusion

This work establishes a strong baseline for real-time polyp segmentation under extreme computational constraints. We present UltraSeg-108K for single-center data and its multi-center variant UltraSeg-130K, which achieve an average Dice of 0.7838 and 0.7926 across five public colonoscopy datasets,

delivering 94% of the performance of a 31M-parameter U-Net while using only 0.1M parameters and running at 90 FPS on a single CPU core. To our knowledge, this is the first model to meet the dual demands of real-time inference and clinically usable accuracy under a ≤ 0.3 M parameter budget, significantly outperforming all existing lightweight alternatives and providing a deployable solution for resource-limited settings.

Our findings also reveal fundamental limitations of conventional model compression in this ultra-lightweight regime. For instance, knowledge distillation from a large teacher model fails to meaningfully improve performance when the student is over 300x smaller, highlighting an inherent capacity gap that cannot be bridged through supervision transfer alone. These insights point to two critical directions for future work: (1) systematically mapping the accuracy–efficiency Pareto frontier for models under 0.3M parameters, and (2) designing pre-training strategies specif-

ically tailored to extremely compact architectures.

More broadly, this study demonstrates that a bottom-up, cross-domain design philosophy, which starts from a proven lightweight backbone and adapts it with precision modules for colonoscopy, can yield highly efficient yet accurate segmentation models. By shifting the focus from pure accuracy toward deployability under strict hardware limits, we provide both a practical pathway and a methodological blueprint for bringing real-time AI assistance to primary-care endoscopy and other minimally invasive imaging domains.

This study establishes a strong performance baseline for real-time polyp segmentation under extreme computational constraints. We present UltraSeg-108K (108K parameters) for single-center scenarios and its multi-center generalization variant, UltraSeg-130K (130K parameters). Experimental results demonstrate that when independently trained and evaluated on five public colonoscopy datasets, the two models achieve mean Dice coefficients of 0.7838 and 0.7926, respectively; under mixed-dataset training, performance further improves to 0.7884 and 0.8038. Notably, with merely 0.1M parameters—approximately 0.4% of the UNet, our models achieve over 94% of the segmentation accuracy of the 31M parameter UNet while delivering real-time inference at 90 FPS on a single-core CPU. To the best of our knowledge, our models significantly outperform all existing lightweight alternatives, offering a viable pathway for AI deployment in resource-constrained environments.

Furthermore, our models exhibit stronger generalization capabilities when trained on diverse data, demonstrating more stable performance on external validation sets and further narrowing the performance gap with heavyweight baselines (UNet-Base). This study also reveals fundamental limitations of conventional model compression paradigms in the ultra-lightweight regime: when the student model is compressed to less than 1/300 of the teacher model size, feature-based knowledge distillation fails to yield substantial improvements, highlighting an inherent capability gap under extreme compression that cannot be bridged by supervised signal transfer alone.

From a broader perspective, this study validates the efficacy of a “bottom-up” cross-domain design paradigm: starting from validated lightweight backbones and achieving efficient yet accurate segmentation through precise module adaptation and structural optimization at extremely low parameter counts. This approach shifts the research focus from pursuing accuracy extremes to ensuring deployability under strict hardware constraints, providing a feasible technical pathway and methodological reference for introducing real-time AI assistance into primary care endoscopic screening and other resource-constrained minimally invasive imaging scenarios.

Declaration of competing interest

The authors declare that they have no known competing financial interests or personal relationships that could have appeared to influence the work reported in this paper.

Code availability

The code for this study is publicly available at <https://github.com/AI-thpremed/ultraseg>.

Acknowledgements

The authors declare that there are no acknowledgements.

References

[1] Ahmir Ahmad, Ana Wilson, Adam Haycock, Adam Humphries, Kevin Monahan, Noriko Suzuki, Siwan Thomas-Gibson, Margaret Vance, Paul Bassett, Kowshika Thiruvilangam, et al. Evaluation of a real-time computer-aided polyp detection system during screening colonoscopy: Ai-detect study. *Endoscopy*, 55(04):313–319, 2023. 1

[2] S Ali, D Jha, N Ghatwary, S Realdon, R Cannizzaro, OE Salem, D Lamarque, C Daul, MA Riegler, KV Anonsen, et al. Polypgen: A multi-center polyp detection and segmentation dataset for generalisability assessment. arxiv 2021. *arXiv preprint arXiv:2106.04463*. 7

[3] Jorge Bernal, Javier Sánchez, and Fernando Vilarino. Towards automatic polyp detection with a polyp appearance model. *Pattern Recognition*, 45(9):3166–3182, 2012. 1

[4] Jorge Bernal, F. Javier Sánchez, Gloria Fernández-Esparrach, Debora Gil, Cristina Rodríguez, and Fernando Vilariño. Cvc-clinicdb, 2015. 7

[5] Debayan Bhattacharya, Konrad Reuter, Finn Behrendt, Lennart Maack, Sarah Grube, and Alexander Schlaefer. Polypnextlstm: a lightweight and fast polyp video segmentation network using convnext and convlstm. *International journal of computer assisted radiology and surgery*, 19(10):2111–2119, 2024. 2

[6] Carlo Biffi, Pietro Salvagnini, Nhan Ngo Dinh, Cesare Hassan, Prateek Sharma, and Andrea Cherubini. A novel ai device for real-time optical characterization of colorectal polyps. *NPJ digital medicine*, 5(1):84, 2022. 1

[7] Hanna Borgli, Vajira Thambawita, Pia H Smedsrød, Steven Hicks, Debesh Jha, Sigrun L Eskeland, Kristin Ranheim Randel, Konstantin Pogorelov, Mathias Lux, Duc Tien Dang Nguyen, et al. Hyperkvasir, a comprehensive multi-class image and video dataset for gastrointestinal endoscopy. *Scientific data*, 7(1):283, 2020. 2

[8] Jia Deng, Wei Dong, Richard Socher, Li-Jia Li, Kai Li, and Li Fei-Fei. Imagenet: A large-scale hierarchical image database. In *2009 IEEE conference on computer vision and pattern recognition*, pages 248–255. Ieee, 2009. 13

[9] Bo Dong, Wenhui Wang, Deng-Ping Fan, Jinpeng Li, Huazhu Fu, and Ling Shao. Polyp-pvt: Polyp segmentation with pyramid vision transformers. *arXiv preprint arXiv:2108.06932*, 2021. 1, 2, 3

[10] Alexey Dosovitskiy, Lucas Beyer, Alexander Kolesnikov, Dirk Weissenborn, Xiaohua Zhai, Thomas Unterthiner, Mostafa Dehghani, Matthias Minderer, Georg Heigold, and Sylvain Gelly. An image is worth 16x16 words: Transformers for image recognition at scale. In *International Conference on Learning Representations*, 2021. 1

[11] Razvan-Gabriel Dumitru, Darius Peteleaza, and Catalin Craciun. Using duck-net for polyp image segmentation. *Scientific reports*, 13(1):9803, 2023. 7, 12

[12] Wilson WB Goh, Kendrick YA Chia, Max FK Cheung, Kalya M Kee, May O Lwin, Peter J Schulz, Minhu Chen, Kaichun Wu, Simon SM Ng, Rashid Lui, et al. Risk perception, acceptance, and trust of using ai in gastroenterology practice in the asia-pacific region: web-based survey study. *JMIR AI*, 3(1):e50525, 2024. 1

[13] Albert Gu and Tri Dao. Mamba: Linear-time sequence modeling with selective state spaces. In *First conference on language modeling*, 2024. 1, 3

[14] Seung-Min Jeong, Seung-Gun Lee, Chae-Lin Seok, Eui-Chul Lee, and Jun-Young Lee. Lightweight deep learning model for real-time colorectal polyp segmentation. *Electronics*, 12(9):1962, 2023. 3

[15] Debesh Jha, Sharib Ali, Krister Emanuelsen, Steven A. Hicks, Vajira Thambawita, Enrique Garcia-Ceja, Michael A. Riegler, Thomas de Lange, Peter T. Schmidt, Håvard D. Johansen, Dag Johansen, and Pål Halvorsen. Kvasir-instrument: Diagnostic and therapeutic tool segmentation dataset in gastrointestinal endoscopy. In *MultiMedia Modeling*, pages 218–229, Cham, 2021. Springer International Publishing. 7

[16] Debesh Jha, Pia H Smedsrød, Michael A Riegler, Pål Halvorsen, Thomas de Lange, Dag Johansen, and

Håvard D Johansen. Kvasir-seg: A segmented polyp dataset. In *International Conference on Multimedia Modeling*, pages 451–462. Springer, 2020. 7

[17] Debesh Jha, Nikhil Kumar Tomar, Vanshali Sharma, Quoc-Huy Trinh, Koushik Biswas, Hongyi Pan, Ritika K Jha, Gorkem Durak, Alexander Hann, Jonas Varkey, et al. Polypdb: A curated multi-center dataset for development of ai algorithms in colonoscopy. *arXiv preprint arXiv:2409.00045*, 2024. 2, 7

[18] Martijn R Jong, Tim GW Boers, Kiki N Fockens, Jelmer B Jukema, Carolus HJ Kusters, Tim JM Jaspers, RAH van Eijck van Heslinga, Floor C Slooter, Maarten R Struyvenberg, Raf Bisschops, et al. Gastronet-5m: A multicenter dataset for developing foundation models in gastrointestinal endoscopy. *Gastroenterology*, 2025. 1, 3

[19] Mehrshad Lalinia and Ali Sahafi. Colorectal polyp detection in colonoscopy images using yolo-v8 network. *Signal, Image and Video Processing*, 18(3):2047–2058, 2024. 1

[20] Ming-De Li, Ze-Rong Huang, Quan-Yuan Shan, Shu-Ling Chen, Ning Zhang, Hang-Tong Hu, and Wei Wang. Performance and comparison of artificial intelligence and human experts in the detection and classification of colonic polyps. *BMC gastroenterology*, 22(1):517, 2022. 1

[21] Xiaomeng Li, Mengyu Jia, Md Tauhidul Islam, Lequan Yu, and Lei Xing. Self-supervised feature learning via exploiting multi-modal data for retinal disease diagnosis. *IEEE Transactions on Medical Imaging*, 39(12):4023–4033, 2020. 3

[22] Long Lin, Guangzu Lv, Bin Wang, Cunlu Xu, and Jun Liu. Polyp-lvt: Polyp segmentation with lightweight vision transformers. *Knowledge-Based Systems*, 300:112181, 2024. 2, 3, 13

[23] Ze Liu, Yutong Lin, Yue Cao, Han Hu, Yixuan Wei, Zheng Zhang, Stephen Lin, and Baining Guo. Swin transformer: Hierarchical vision transformer using shifted windows. In *Proceedings of the IEEE/CVF international conference on computer vision*, pages 10012–10022, 2021. 3

[24] Eileen Morgan, Melina Arnold, A Gini, V Lorenzoni, CJ Cabasag, Mathieu Laversanne, Jerome Vignat, Jacques Ferlay, Neil Murphy, and Freddie Bray. Global burden of colorectal cancer in 2020 and 2040: incidence and mortality estimates from globocan. *Gut*, 72(2):338–344, 2023. 1

[25] Zhiyuan Niu, Zhuo Deng, Weihao Gao, Shurui Bai, Zheng Gong, Chucheng Chen, Fuju Rong, Fang Li, and Lan Ma. Fnexter: a multi-scale feature fusion network based on convnext and transformer for retinal oct fluid segmentation. *Sensors*, 24(8):2425, 2024. 3

[26] Xing-Liang Pan, Ju-Rong Ding, Xia Li, Shuo Liu, Jie Wang, Bo Hua, Guo-Zhi Tang, and Chang-Hua Zhong. Msbp-net: A multi-scale boundary prediction network for automated polyp segmentation. *Pattern Recognition*, 170:112101, 2026. 2

[27] Adriana Romero, Nicolas Ballas, Samira Ebrahimi Kahou, Antoine Chassang, Carlo Gatta, and Yoshua Bengio. Fitnets: Hints for thin deep nets. *arXiv preprint arXiv:1412.6550*, 2014. Published at ICLR 2015. 6

[28] Olaf Ronneberger, Philipp Fischer, and Thomas Brox. U-net: Convolutional networks for biomedical image segmentation. In *Medical Image Computing and Computer-Assisted Intervention–MICCAI 2015: 18th International Conference, Munich, Germany, October 5–9, 2015, Proceedings, Part III 18*, pages 234–241. Springer, 2015. 1, 3

[29] Jiacheng Ruan, Mingye Xie, Jingsheng Gao, Ting Liu, and Yuzhuo Fu. Ege-unet: an efficient group enhanced unet for skin lesion segmentation. In *International conference on medical image computing and computer-assisted intervention*, pages 481–490. Springer, 2023. 2, 3, 4

[30] Sofia Saraiva, Isadora Rosa, Ricardo Fonseca, and António Dias Pereira. Colorectal malignant polyps: a modern approach. *Annals of Gastroenterology*, 35(1):17, 2021. 1

[31] T. H. Son and P. D. Hung. Polyps segmentation in colonoscopy images using SegFormer transformer. In *International Conference on Artificial Intelligence and Soft Computing*, pages 368–378, Cham, June 2024. Springer Nature Switzerland. 7, 12

[32] Fiseha B Tesema, Alejandro Guerra Manzanares, Tianxiang Cui, Qian Zhang, Moses Solomon, and Sean He. Lgps: A lightweight gan-based approach for polyp segmentation in colonoscopy images. *arXiv preprint arXiv:2503.18294*, 2025. 2, 3

[33] Aling Wang, Jiahao Mo, Cailing Zhong, Shaohua Wu, Sufen Wei, Binqi Tu, Chang Liu, Daman Chen, Qing Xu, Mengyi Cai, et al. Artificial intelligence-assisted detection and classification of colorectal polyps under colonoscopy: a systematic review and meta-analysis. *Annals of Translational Medicine*, 9(22):1662, 2021. 1

[34] Shuo Wang, Yue Zhu, Xiao Luo, Zhen Yang, Yichao Zhang, Ping Fu, Chen Liu, and Yanjun Guo. Knowledge extraction and distillation from large-scale image-text colonoscopy records leveraging large language and vision models. *arXiv preprint arXiv:2310.11173*, 2023. 3

[35] Wenhai Wang, Enze Xie, Xiang Li, Deng-Ping Fan, Kaitao Song, Ding Liang, Tong Lu, Ping Luo, and Ling Shao. Pyramid vision transformer: A versatile backbone for dense prediction without convolutions. In *Proceedings of the IEEE/CVF international conference on computer vision*, pages 568–578, 2021. 3

[36] Wenhai Wang, Enze Xie, Xiang Li, Deng-Ping Fan, Kaitao Song, Ding Liang, Tong Lu, Ping Luo, and Ling Shao. Pvt v2: Improved baselines with pyramid vision transformer. *Computational visual media*, 8(3):415–424, 2022. 3, 13

[37] Ziyang Wang, Jian-Qing Zheng, Yichi Zhang, Ge Cui, and Lei Li. Mamba-unet: Unet-like pure visual mamba for medical image segmentation. *arXiv preprint arXiv:2402.05079*, 2024. 3

[38] Junde Wu, Ziyue Wang, Mingxuan Hong, Wei Ji, Huazhu Fu, Yanwu Xu, Min Xu, and Yueming Jin. Medical sam adapter: Adapting segment anything model for medical image segmentation. *Medical Image Analysis*, 102, 2025. 3

[39] Zhaohu Xing, Tian Ye, Yijun Yang, Guang Liu, and Lei Zhu. Segmamba: Long-range sequential modeling mamba for 3d medical image segmentation. In *International conference on medical image computing and computer-assisted intervention*, pages 578–588. Springer, 2024. 3

[40] Hanwen Xu, Naoto Usuyama, Jaspreet Bagga, Sheng Zhang, Rajesh Rao, Tristan Naumann, Cliff Wong, Zelalem Gero, Javier González, Yu Gu, et al. A whole-slide foundation model for digital pathology from real-world data. *Nature*, 630(8015):181–188, 2024. 3

[41] Jiahao Xu and Lyuyang Tong. Lb-unet: A lightweight boundary-assisted unet for skin lesion segmentation. In *International Conference on Medical Image Computing and Computer-Assisted Intervention*, pages 361–371. Springer, 2024. 2, 3, 4